JOURNAL OF ENVIRONMENTAL SCIENCES 124 (2023) 130–138

Available online at www.sciencedirect.com

ScienceDirect

www.elsevier.com/locate/jes

JES JOURNAL OF ENVIRONMENTAL SCIENCES

www.jesc.ac.cn

Insight into the interaction between trimethoprim and soluble microbial products produced from biological wastewater treatment processes

Runze Xu, Fang Fang, Longfei Wang, Jingyang Luo, Jiashun Cao*

Key Laboratory of Integrated Regulation and Resource Development on Shallow Lakes, Ministry of Education, College of Environment, Hohai University, Nanjing 210098, China

ARTICLE INFO

Article history:
Received 19 September 2021
Revised 10 November 2021
Accepted 10 November 2021
Available online 1 February 2022

Keywords:
Activated sludge process
Interaction mechanism
Antibiotics
Soluble microbial products (SMP)
Spectral methods

ABSTRACT

Soluble microbial products (SMPs), dissolved organic matter excreted by activated sludge, can interact with antibiotics in wastewater and natural water bodies. Interactions between SMPs and antibiotics can influence antibiotic migration, transformation, and toxicity but the mechanisms involved in such interactions are not fully understood. In this study, integrated spectroscopy approaches were used to investigate the mechanisms involved in interactions between SMPs and a representative antibiotic, trimethoprim (TMP), which has a low biodegradation rate and has been detected in wastewater. The results of liquid chromatography-organic carbon detection-organic nitrogen detection indicated that the SMPs used in the study contained 15% biopolymers and 28% humic-like substances (based on the total dissolved organic carbon concentration) so would have contained sites that could interact with TMP. A linear relationship of fluorescent intensities of tryptophan protein-like substances in SMP was observed (R^2>0.99), indicating that the fluorescence enhancement between SMP and TMP occurred. Fourier-transform infrared spectroscopy and X-ray photoelectron spectroscopy indicated that carboxyl, carbonyl, and hydroxyl groups were the main functional groups involved in the interactions. The electrostatic and π-π interactions were discovered by the UV-vis spectra and ^{1}H nuclear magnetic resonance spectra. Structural representations of the interactions between representative SMP subcomponents and TMP were calculated using density functional theory, and the results confirmed the conclusions drawn from the ^{1}H nuclear magnetic resonance spectra. The results help characterize SMP–TMP complexes and will help understand antibiotic transformations in wastewater treatment plants and aquatic environments.

Introduction

Biological treatment processes are widely used in wastewater treatment plants (WWTPs). The effluents of WWTPs contain complex mixtures of organic compounds, including residual refractory compounds, intermediates, and soluble microbial products (SMPs). SMPs include a wide range of compounds such as proteins (PN), polysaccharides (PS), and humic acid (HA), that are released during microbial biosynthesis and lysis (Laspidou and Rittmann, 2002). The high molecular weights (MW) and complex structures of SMPs make it difficult for SMPs to be biodegraded (Wang et al., 2018;

* Corresponding author.
E-mail: ffang65@hhu.edu.cn (F. Fang).

https://doi.org/10.1016/j.jes.2021.11.010

Yang et al., 2018). SMPs can therefore be the most important components of the chemical oxygen demand (COD) of WWTP effluent and can be discharged into natural aquatic environments (Yang et al., 2018). The diverse functional groups (*e.g.*, amino, carbonyl, carboxyl, hydroxyl, ester, and phenol groups) in the components of SMPs could interact with various pollutants in wastewater and natural aquatic environments (Duan et al., 2013; Zhou et al., 2017a). In practice, adsorption between multiple functional groups and organic pollutants usually occurs (Li and Yu, 2014). For example, the carboxyl group is negatively charged in a neutral pH solution and can interact with positively charged cations through electrostatic interactions (Ozdemir et al., 2003). Hydrophobic functional groups such as aliphatic groups, aromatic groups, and hydrophobic regions in carbohydrates may be involved in hydrophobic interactions (Huangfu et al., 2019). Abundant polar functional groups may act as hydrogen-bond donors (Zhao et al., 2014).

It has been found in previous studies that SMPs can interact with heavy metals through multiple mechanisms. For example, SMPs have been found to bind to soluble ferric iron under acidic conditions and inhibit pyrite oxidation. SMPs have also been found to strongly interact with (in decreasing interaction strength) Cu^{2+}, Al^{3+}, and Fe^{3+} and to markedly affect heavy metal speciation in effluents (Wu et al., 2015; Xu et al., 2015). The complex interactions between SMPs and ZnO nanoparticles have been found to intensify membrane fouling (Mei et al., 2014). Besides heavy metals, antibiotics have been widely detected in wastewater and natural water bodies (Thiebault, 2020). However, our understanding of interactions between SMPs and antibiotics is limited.

The potential risks posed by antibiotics to ecosystems and human health are of public concern (Su et al., 2021; Zumstein and Helbling, 2019). During biological wastewater treatment processes, SMPs released from activated sludge can interact with antibiotics in the wastewater. The SMP–antibiotic complexes may then affect the removal efficiencies of antibiotics during biological and tertiary wastewater treatment processes (Hernandez-Ruiz et al., 2012). The complexes can be discharged into the natural environment and remain for a long time because of their bio-refractory properties. Interactions between SMPs and antibiotics may therefore affect the toxicities, migration, and environmental fates of antibiotics (Lee et al., 2014). It is therefore important to improve our understanding of the mechanisms involved in interactions between SMPs and antibiotics. Trimethoprim (TMP), a common antibiotic, is a bacteriostatic antibiotic derived from trimethoxybenzylpyrimidine that has been widely used since 1968 (Thiebault, 2020). TMP has been detected in the influents of WWTPs all over the world at concentrations between 20 ng/L and 72.9 μg/L (Thiebault, 2020). TMP is poorly biodegraded, so can accumulate in treated wastewater and natural environments (Shahriar et al., 2021). TMP was therefore selected as the target antibiotic for this study.

In this study, the mechanisms involved in interactions between SMPs and TMP were investigated. The components of SMPs extracted from activated sludge were characterized by liquid chromatography-organic carbon detection-organic nitrogen detection (LC-OCD-OND). Then, integrated spectroscopy methods (UV-vis spectroscopy, three-dimensional excitation-emission matrix (3D-EEM) fluorescence spectroscopy, Fourier-transform infrared (FTIR) spectroscopy, X-ray photoelectron spectroscopy (XPS), and ^{1}H nuclear magnetic resonance (^{1}H NMR) spectroscopy) were used to elucidate the possible mechanisms involved in interactions between the SMPs and TMP. Conformational changes, the fluorescence properties, the main functional groups, and donor–acceptor interactions were assessed using the results of the integrated spectroscopic analyses. The optimized structures of the SMP–TMP complexes were calculated using density functional theory (DFT). The results were expected to provide useful insights into SMP–TMP interactions.

1. Materials and methods

1.1. Reactor operation

A sequencing batch reactor (SBR) with an effective volume of 9 L was used. The 6 hr SBR operating cycle consisted of five periods, filling (10 min), aerating (310 min), sinking (20 min), draining (10 min), and idle (10 min). The hydraulic retention time (HRT) was 12 hr. Mixed liquor was discharged each day to maintain a solid retention time (SRT) of 15 days. The SBR temperature was not controlled, so was at the ambient temperature of 20–25°C. The oxygen concentration (>4 mg/L) during the aerating period was maintained using an air pump.

Seed sludge was obtained from a municipal WWTP in Nanjing City, China. The sludge was washed twice with deionized water and then passed through a 0.6 mm filter to remove particles. The initial mixed liquor suspended solids (MLSS) concentration in the mixed liquor in the SBR was 4000 mg/L.

The synthetic wastewater contained sodium acetate (1000 mg COD/L) to act as the sole carbon source for microbial growth, NH_4Cl (20 mg N/L), KH_2PO_4 (10 mg P/L), $MgSO_4$ (15 mg/L), $CaCl_2$ (20 mg/L), $FeSO_4$ (15 mg/L), and trace elements (1 mL/L of a mixed trace element solution), as previously described by Fang et al. (2015). The influent was adjusted to pH 7.0 ± 0.2 by adding NaOH (1 mol/L) or HCL (1 mol/L). Sodium acetate was chosen to be the carbon source to eliminate the interference of influent on SMPs. SMPs were therefore the dominant form of dissolved organic carbon in the SBR effluent at the end of the 6 hr cycle.

1.2. SMP analysis

Each mixed liquor sample collected from the SBR effluent at the end of the 6 hr cycle was centrifuged for 15 min at 12,000 r/min and then passed through a 0.45 μm acetate cellulose membrane filter to give a solution containing the SMPs (Xie et al., 2019). The polysaccharide concentration in the SMP solution was determined using the anthrone method using glucose as a standard (Sheng et al., 2005). The protein and humic compound concentrations in the SMP solution were determined using the corrected Lowry method using egg albumin and humic acid, respectively, as standards (Raunkjær et al., 1994). The SMPs consisted of 2.21 ± 0.16

mg COD/L PS, 1.76 ± 0.17 mg COD/L PN, and 7.11 ± 0.48 mg COD/L HA. The SMP samples were also analyzed using an LC-OCD-OND instrument (DOC-Labor, Karlsruhe, Germany) using a method described by Jacquin et al. (2017). The LC-OCD-OND method separates soluble organic matter into five types (*i.e.*, biopolymers, humic substances, building blocks, low-molecular-weight (LMW) acids, and LMW neutral compounds) and allows each type to be quantified (Jacquin et al., 2017).

1.3. *Binding experiments*

The mechanisms involved in interactions between SMPs and TMP were explored using TMP (standard G1719036; Aladdin, USA) at concentrations in the range 0.1–10 mg/L. The TMP concentration range was much higher than the TMP concentrations that have been found in natural aquatic environments because interactions between TMP at low concentrations (<100 μg/L) and SMPs cannot readily be detected. The actual concentrations and effects of refractory organic substances (*e.g.*, TMP) in natural aquatic environments may also be much higher than the detected concentrations because of accumulation effects. TMP solutions at concentrations of 0.1, 1, 5, and 10 mg/L for use in the binding experiments were prepared by diluting the stock TMP solution (in methanol) with deionized water. A 45 mL aliquot of SMP-containing solution was added to each of a series of beakers. A TMP solution at a specified concentration was then added to each beaker to give a final volume of 50 mL. The solution in each beaker was immediately mixed well and subjected to UV-vis spectroscopy and 3D-EEM fluorescence spectroscopy. An Alpha-1506 UV-vis spectrometer (PuYuan, China) was used to acquire UV-vis spectra in the wavelength range 200–700 nm. The 3D-EEM spectra were acquired using an F-7000 fluorescence spectrophotometer (Hitachi High-Technologies, Tokyo, Japan) using a method described by Xie et al. (2019).

The functional groups involved in SMP–TMP interactions were investigated by subjecting freeze-dried pristine SMPs and freeze-dried complexes formed in a mixture of the SMPs and 10 mg/L TMP (SMP_10-TMP) to FTIR spectroscopy, XPS, and ^{1}H NMR spectroscopy. A high TMP concentration (10 mg/L) was used to overcome noise in the spectra acquired using the instruments (the FTIR spectrometer, XPS instrument, and ^{1}H NMR spectrometer). A vacuum freeze dryer (Labconco, USA) was used to freeze-dry each prepared solution. The dried samples were analyzed using a Nexus 870 FTIR spectrometer (Thermo Nicolet, USA), a PHI 5000 XPS instrument (VersaProbe, USA), and a DRX500 ^{1}H NMR spectrometer (Bruker, Billerica, MA, USA). The FTIR spectroscopy and XPS methods described by Feng et al. (2018) were used. The method of ^{1}H NMR spectra was reported by Kavita et al. (2013).

Structural data for TMP and three representative SMP components (alginate, fulvic acid (FA), and tryptophan) were obtained from the PubChem open chemistry database (https://pubchem.ncbi.nlm.nih.gov/). Interaction structures of SMP–TMP complexes at minimum total steric energy were calculated using the MM2 Minimize function. DFT calculations were performed using ChemOffice Professional V19.0 software (PerkinElmer, Waltham, MA, USA).

2. Results and discussion

2.1. *Characteristics of SMP components*

The LC-OCD-OND system separated the soluble organic matter into five components, *i.e.*, biopolymers, humic substances, building blocks, LMW acids, and LMW neutral compounds. Among them, biopolymers are polysaccharides and proteins (Jacquin et al., 2017). As shown in Appendix A **Table S1**, biopolymers, humic-like substances, and LMW neutral compounds were the main SMP components, contributing 15%, 28%, and 51%, respectively, of the total dissolved organic carbon. The biopolymers and humic-like substances in SMPs can contain sites that can adsorb organic matter (Chakraborty et al., 2019; Xu et al., 2018). For example, complex interactions, such as hydrophobic/hydrophilic interactions, electrostatic interactions, and van der Waals interactions, may occur in an aqueous solution containing organic matter and proteins (Chakraborty et al., 2019). FAs can interact with the antibiotic sulfamethazine through hydrophobic interactions and ancillary π–π conjunction contributions caused by aromatic rings in FA and sulfamethazine forming stacks to give stable FA–sulfamethazine complexes (Xu et al., 2018). The components of SMPs may therefore contain sites to which TMP can bind. The mechanisms involved in the interactions needed to be explored using spectral methods.

2.2. *Investigating conformational changes in SMPs caused by SMP–TMP interactions by UV-vis spectroscopy*

Conformational changes in SMPs caused by interactions with TMP at different concentrations were detected by UV-vis spectroscopy. As shown in **Fig. 1a**, there were distinctive TMP peaks at 205 and 278 nm. The peaks at 205 and 278 nm were assigned to the ($^1L_a < {}^1A$) transition of the benzene ring and the $\pi \rightarrow \pi^*$ transition of the benzene ring derivative in TMP, respectively (Aly et al., 2016; Mal et al., 2017). The UV-vis spectrum of the pristine SMPs contained one peak at 206 nm, which was similar to the TMP peak (**Fig. 1b**). Interactions between the SMPs and TMP caused the intensity of the 206 nm peak to increase as the TMP concentration increased and the 278 nm peak to become red-shifted to 287 nm. This indicated that the benzene ring played an important role in interactions between the SMPs and TMP.

To magnify the change of UV-vis spectral response to the addition of TMP, the data in **Fig. 1a** were subtracted from that in **Fig. 1b** according to TMP concentrations (Habibul and Chen, 2018). As shown in **Fig.1c**, the intensities of the 205 and 287 nm peaks both decreased as more TMP interacted with the SMPs. These results suggested that π-bonding interactions between the SMPs and the benzene ring in TMP occurred. This conclusion was further verified by subsequent NMR analyses.

2.3. *Fluorescence enhancement caused by SMP–TMP interactions*

Five fluorescence peaks (labeled I–V) were found for the pristine SMPs, as shown in **Fig. 2a**. The peak positions and fluorescence intensities are shown in Appendix A **Table S2**. Peak

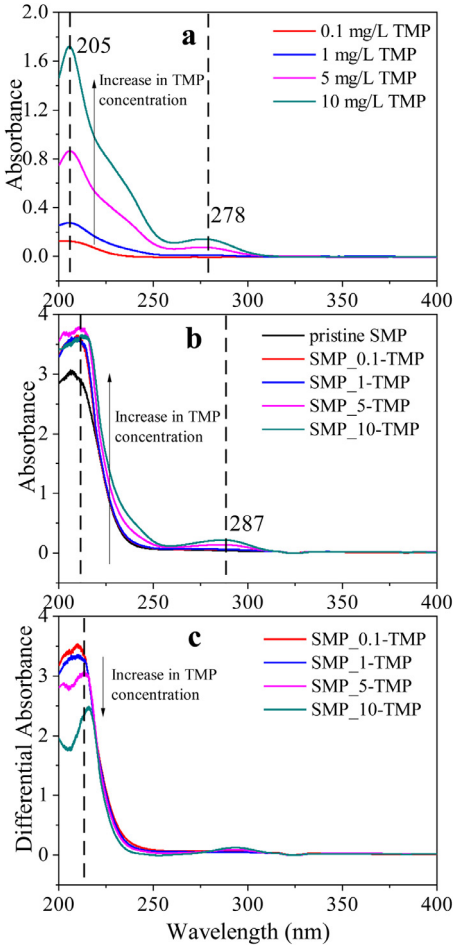

Fig. 1. – UV-vis spectra of (a) trimethoprim (TMP) at different concentrations, (b) soluble microbial products (SMP) reacting with TMP at different concentrations, and (c) differential log-transformed absorption spectra of SMP with TMP at different concentrations.

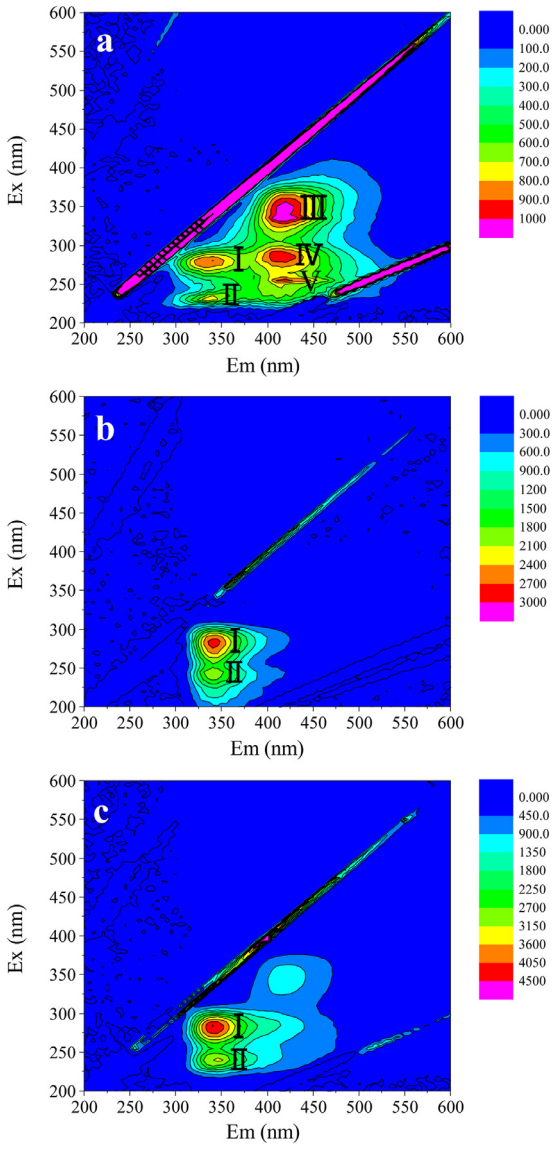

Fig. 2. – Three-dimensional excitation-emission matrix spectra of samples: (a) the pristine soluble microbial products, (b) 10 mg/L trimethoprim, and (c) the complexes formed between the soluble microbial products and 10 mg/L trimethoprim.

I (Ex/Em = 280/340 nm) was assigned to tryptophan protein-like substances. Peak II (Ex/Em = 230/355 nm) was assigned to the tryptophan amino acid. Peak III (Ex/Em = 335/415 nm), peak IV (Ex/Em = 285/410 nm), and peak V (Ex/Em = 255/420 nm) were assigned to humic acid-like substances (Chen et al., 2003; Li et al., 2020). As shown in Fig. 2b, the two main fluorescence peaks for TMP were the same as peaks I and II for the SMPs, indicating that the TMP structure was similar to the tryptophan protein-like substances in the SMPs. However, interactions between the SMPs and 10 mg/L TMP caused the fluorescence intensities of peaks I and II to increase (Fig. 2c).

The fluorescence intensity of peak I (Ex/Em = 280/340 nm) for the complex between the SMPs and 10 mg/L TMP was stronger than the sum of the separate fluorescence intensities of peak I for the pristine SMPs and 10 mg/L TMP. The fluorescence intensity of peak II (Ex/Em = 230/355 nm) followed the same pattern because of the fluorescence enhancement effect. Fluorescence enhancement is generally caused by energy transfer through dipole–dipole interactions between a donor and an acceptor (Yang et al., 2010). The fluorescence enhancement effect was assessed over a large TMP concentration range (1–10 mg/L) using a dose–response graph (using $\Delta F/F_0$, where F_0 is the fluorescence intensity before adding the TMP dose and ΔF is the change in fluorescence intensity caused by adding the TMP dose) (Aparna et al., 2019). Linear relationships were found for both peaks I and II (Fig. 3), indicating that interactions between the SMPs and TMP caused fluorescence enhancement and that tryptophan protein-like substances in the SMPs controlled the SMP–TMP interactions. Fluorescence quenching was found to be caused by interactions between SMPs and metal ions in a previous study (Xu et al., 2015). Such a difference resulted from the different structures and properties of metal ions and TMP. The fluorescence enhancement that occurred indicated that interactions between

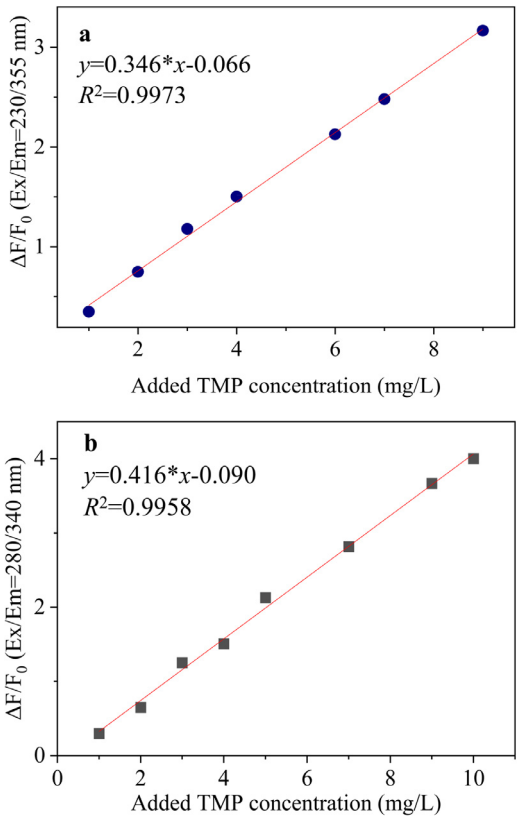

Fig. 3. – Dose–response graphs for the soluble microbial products after trimethoprim (TMP) had been added. (a) Ex/Em = 230/355 nm. (b) Ex/Em = 280/340 nm.

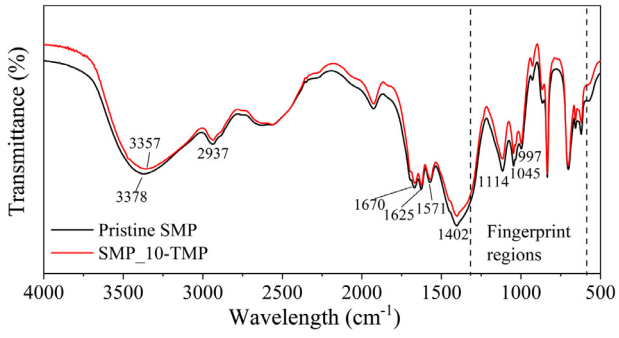

Fig. 4. – Fourier-transform infrared spectra of the pristine soluble microbial products (SMP) and the complexes formed between the SMP and 10 mg/L trimethoprim (TMP).

the SMPs and TMP could change the molecular structures of the SMPs and TMP and therefore increase the fluorescence quantum yields (Yamashita and Jaffe, 2008).

2.4. *Functional groups governed the SMP–TMP interactions*

The pristine SMPs and the complexes formed between the SMPs and 10 mg/L TMP were characterized by FTIR spectroscopy (Fig. 4). Absorption peaks between 4000 and 500 cm^{-1} indicated that the SMP components were complex and similar to the compositions of extracellular polymeric substances (EPSs) found in a previous study (Song et al., 2014). The spectrum for the pristine SMPs contained a broad peak at 3378 cm^{-1} corresponding to O–H stretching vibrations in polysaccharides and H-bonding between N–H and O–H groups in proteins and polysaccharides (Sajjad and Kim, 2015). A peak at 2937 cm^{-1} was attributed to C–H stretching vibrations (Hyun-Chul and Dempsey, 2008). Peaks at 1670 and 1625 cm^{-1} were assigned to C=O stretching vibrations in protein-like substances (parts of the amide I band for the secondary protein structure). A peak at 1571 cm^{-1} was assigned to interactions between C–N and N–H bonds in C–N–H groups in the amide II band. A peak at 1402 cm^{-1} indicated the presence of an amide III band (Maruyama et al., 2001). Three peaks between 1114 and 997 cm^{-1} were assigned to C–O–C ring and C–O stretching vibrations, indicating the presence of polysaccharide-like substances (Kimura et al., 2005).

After SMPs interacted with 10 mg/L TMP, the FTIR spectrum of the complex between SMPs and 10 mg/L TMP changed. The peak positions in the two spectra were almost identical but the absorption intensities were slightly different, possibly because of the relatively low concentrations of the SMP compounds. The intensity of the peak at 3378 cm^{-1} was lower for the complexes than the pristine SMPs and the position had slightly shifted to 3357 cm^{-1} in the spectrum for the complexes because of structural changes in the hydroxyl functional groups (O–H) in the SMPs (Duan et al., 2013). The intensities of the peaks at 1670–1571 and 1402 cm^{-1} were slightly lower for the complexes than the pristine SMPs, indicating that the amide I, II, and III bands for the proteins contributed to SMP–TMP interactions and carbonyl groups (C=O) also made important contributions (Wang et al., 2019). Interactions between the SMPs and TMP also decreased the intensities of the three peaks between 1114 and 997 cm^{-1}, indicating that the carboxyl groups (C–O) in the polysaccharide-like substances in the SMPs were involved in the SMP–TMP interactions (Kimura et al., 2005). The FTIR spectroscopy results indicated that functional groups including O–H, C–O, and C=O in the SMPs governed the interactions between the SMPs and TMP. These changes in the functional groups were supported by the XPS results.

The high-resolution XPS spectra scans of C1s and O1s were employed to determine the changes of functional groups between the pristine SMP and the complex between SMP and 10 mg/L TMP. The C1s and O1s peaks in the pristine SMP spectrum and in the spectrum for the complexes formed between the SMPs and 10 mg/L TMP are shown in Fig. 5. The assignments and integration results for these XPS spectral bands are shown in Table 1. The pristine SMP spectrum contained four C1s peaks (Fig. 5**a**). The peak at 284.3 eV, which was attributed to C–(C,H) from the side chains of lipids or amino acids, presented the largest percent (48.14%). The peaks at 284.9 and 285.9 eV were assigned to C–(O,N) in alcohol, amine, and ether amide groups. The peak at 287.2 eV represented C=O or O–C–O from carboxylate, carbonyl, amide, acetal or hemiacetal groups, which accounted for the lowest percent (3.38%) (Song et al., 2014). The O1s peak in the pristine SMP spectrum was resolved into two peaks (Fig. 5**c**). The peak at 530.7 eV was assigned to O=C in carboxylate, carbonyl, ester, and amide groups and contributed 30.27%. The second O1s

Table 1 – Binding energies (eV), assignments, and quantization of the bands in the X-ray photoelectron spectra of the pristine soluble microbial products and the complexes between the soluble microbial products (SMP) and 10 mg/L trimethoprim (TMP).

Element	SMP peak (eV)	atomic (%)	Complex between SMP and 10 mg/L TMP peak (eV)	atomic (%)	Assignments
C 1s	284.3	48.14	284.2	47.27	C-(C,H)
C 1s	284.9	35.14	285.1	18.20	C-(O,N)
C 1s	285.9	13.34	286.2	7.79	C-(O,N)
C 1s	287.2	3.38	287.7	7.44	C=O, O-C-O
C 1s	-	-	288.7	4.98	O=C-OH, O=C-OR
C 1s	-	-	289.2	13.87	Carboxyl or ester group
O 1s	530.7	30.27	530.7	33.33	C=O
O 1s	531.9	69.73	531.5	66.67	C-O-C, C-O-H

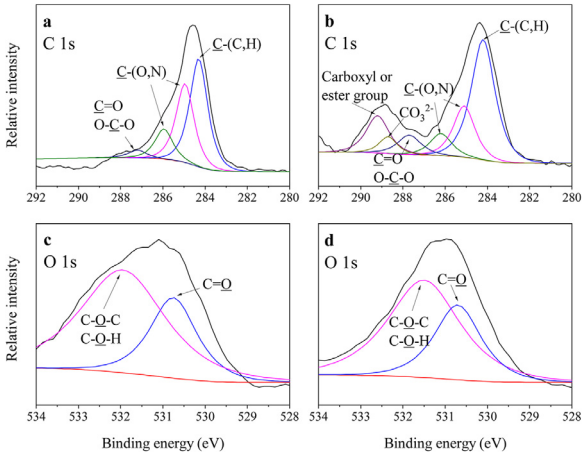

Fig. 5. – X-ray photoelectron spectra of (a and c) the pristine soluble microbial products and (b and d) the complexes formed between the soluble microbial products and 10 mg/L trimethoprim.

peak at 531.9 eV was attributed to C–O–C and C–O–H bonds in alcohol, hemiacetal, and acetal groups (Sun et al., 2011).

Interactions between the SMPs and TMP caused two new peaks to appear in the C1s spectrum (Fig. 5b). The new peak at 288.7 eV, which was attributed to O=C–OH, O=C–OR, showed the lowest percent (4.98%) (Zhou et al., 2017b). The peak at 289.2 eV was assigned to carboxyl or ester groups (Song et al., 2014). This indicated that the TMP formed additional functional groups (O=C–OH, O=C–OR, carboxyl, and ester groups) with the SMPs. The C1s peak at 284.30 eV was slightly transformed into 284.20 eV due to the decline of electronic density round C from C–(C,H). Furthermore, the C1s peaks at 284.9, 285.9, and 287.2 eV were shifted to 285.10, 286.2, and 287.70 eV, respectively, by adding TMP because the electron density around C in C–(O,N) or C=O groups would have increased. The O1s peak at 531.9 eV was shifted to 531.5 eV by adding TMP, indicating that the electron clouds around carbon or hydrogen atoms were transferred from the oxygen atom (Song et al., 2014). These shifts implied that the interactions between the SMPs and TMP were governed by O–H, C–O, and C=O groups in the SMPs, which agreed with the FTIR spectroscopy results.

2.5. *Interactions between hydrogen donors and acceptors in the SMP–TMP complexes*

The ^{1}H NMR spectra of the pristine SMPs and SMP–TMP complexes are shown in Appendix A **Fig. S1**. Peaks in the pristine SMP ^{1}H NMR spectrum at 3.7–3.4 ppm were assigned to hydrogen atoms in –OH groups in PS and PN (Mishra et al., 2011). A peak at 4.70 ppm was assigned to the solvent (D_2O).

Additional peaks were found in the ^{1}H NMR spectrum of the SMP–TMP complexes. A weak peak at 7.59 ppm was attributed to the aromatic ring structure of TMP and a peak at 6.52 ppm was assigned to aromatic protons in TMP (Ganesh and Elango, 2012). Stretching of the N–H group in TMP gave a peak at 1.81 ppm (Mishra et al., 2011). Extensive changes between 3.7 and 3.2 ppm were caused by interactions between the SMPs and TMP. A strong peak at 3.73 ppm was assigned to the $-CH_2$ group connecting the pyrimidine ring with the phenyl ring in TMP (Ganesh et al., 2012). These results implied that electrostatic interaction was one of the driving forces for the interaction between SMP and TMP, in which the H-donor-acceptor and π–π interaction were also involved.

The ^{1}H NMR spectroscopy results were validated by calculating the structures of SMP–TMP complexes with minimum total steric energy, and the results are shown in Fig. 6. Three representative constituents of the SMPs including tryptophan (Tryp), fulvic acid (FA), and alginate (Alg) were selected for interactions with TMP. The minimum total steric energy for Tryp–TMP, FA–TMP, and Alg–TMP complexes were 11.6624, 44.1349, and 20.5749 kcal/mol, respectively. H-donor-acceptor interactions governed the interactions in the Tryp–TMP and Alg–TMP complexes but π–π interactions dominated the interactions between FA and TMP. Similarly, Xu et al. (2018) also found that the aromatic ring in the antibiotic sulfamethazine was stacked with aromatic rings in FAs. These results were consistent with the NMR spectroscopy results

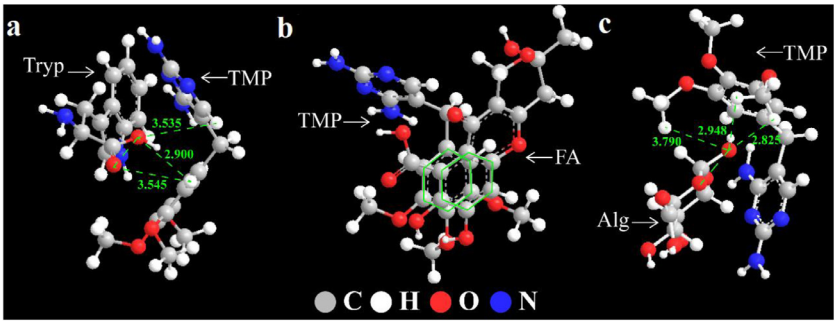

Fig. 6. – Most stable structures for interactions between trimethoprim (TMP) and components of the soluble microbial products (a) tryptophan (Tryp), (b) fulvic acid (FA), and (c) alginate (Alg).

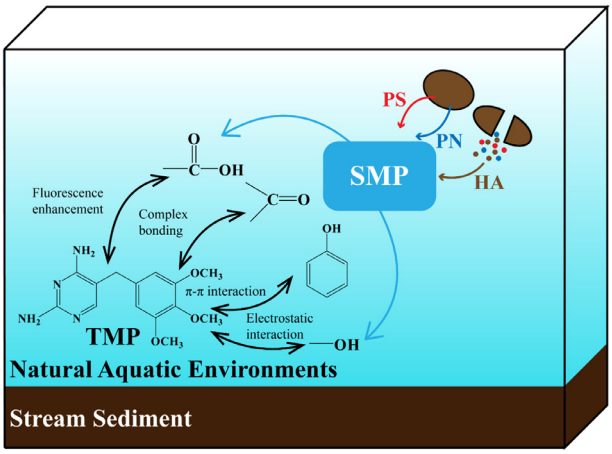

Fig. 7. – Mechanisms involved in the interactions between the soluble microbial products (SMP) and trimethoprim (TMP). PS: polysaccharides, PN: proteins, HA: humic acid.

and indicated the importance of H-donor-acceptor and π–π interactions.

2.6. SMP–TMP interaction mechanisms

The mechanisms involved in SMP–TMP interactions are shown in Fig. 7. The UV-vis and ^{1}H NMR spectroscopy results indicated that both π–π interaction and electrostatic interaction were involved in TMP binding to the SMPs (Fig. 1). The fluorescence enhancement effect of tryptophan protein-like substances found from the 3D-EEM spectra indicated that tryptophan protein-like substances in the SMPs dominated the SMP–TMP interactions (Figs. 2 and 3). The main functional groups involved in SMP–TMP interactions were carboxyl, carbonyl, and hydroxyl groups in the SMPs, as shown by the FTIR spectroscopy and XPS results (Figs. 4 and 5). The integrated spectroscopy methods allowed the mechanisms involved in SMP–TMP interactions involving fluorescence enhancement, π–π interactions, and electrostatic interactions to be elucidated.

Electrostatic interactions and complex formation involved in SMP–TMP interactions have also been found to occur in interactions between EPSs and common antibiotics such as sulfamethazine and tetracycline (Song et al., 2014; Xu et al., 2013). However, fluorescence quenching that generally occurs because of interactions between EPSs and antibiotics did not occur in the SMP-TMP interaction. This might be caused by the specific structure of TMP and the different compositions between SMPs and EPSs. For example, tyrosine protein-like substances were not detected from the 3D-EEM spectra of the SMPs we used, but tyrosine protein-like substances governed the interaction between EPSs and sulfamethazine (Xu et al., 2013).

Other antibiotics discharged in wastewater may also interact with SMPs secreted by activated sludge in biological WWTPs. These interactions between SMPs and antibiotics may affect the distributions, migration, bioavailability, and toxicities of these antibiotics. For example, SMPs released from a membrane bioreactor were found to play important roles in membrane fouling and to interact with antibiotics when the reactor was used to treat pharmaceutical wastewater (Ng et al., 2016). Interactions between SMPs and antibiotics may affect biodegradation of antibiotics during biological treatment and even affect subsequent tertiary wastewater treatment processes such as filtration, treatment using a membrane biological reactor enhanced with powdered activated carbon, and ozonation–UV treatment (Echevarria et al., 2019; Oberoi et al., 2019; Quang Viet et al., 2019). After entering a source of drinking water, complexes between SMPs and antibiotics could affect the formation of disinfection byproducts during disinfection in a drinking water treatment plant (Wu et al., 2019).

The mechanisms involved in interactions between SMPs and TMP identified here improve our understanding of SMP–TMP complexes and will improve our ability to utilize such interactions to decrease membrane fouling (Kimura et al., 2005), enhance the performances of biological wastewater treatment systems, and control antibiotic distribution and migration in aquatic environments (Oberoi et al., 2019). We found that fluorescence enhancement occurred and identified key functional groups and mechanisms involved in interactions between SMPs and TMP, but interactions between key substances in SMPs and antibiotics should be quantitatively explored further to gain further insights into the effects of SMPs on antibiotics (*e.g.*, accelerating or decelerating biodegradation). Further micro-scale investigations should be performed in the future. This will allow strategies for decreasing the toxicities of

antibiotic residues in natural environments using SMPs to be established.

3. Conclusion

In this study, the interaction mechanism between TMP and SMP released by activated sludge was investigated. Biopolymers and humic substances in SMP were found to provide the foundation for their combination with organic matters like TMP. SMP was demonstrated to be capable of binding with TMP and had essential effects on the mobilization and dispersion of TMP. The SMP-TMP interaction mechanisms including fluorescence enhancement effect, complexing bonding, electrostatic interactions, and π-π interaction were elucidated. These results can provide useful information about the interaction mechanism between SMP and antibiotics and the fates of antibiotics in WWTP and aqueous environments.

Acknowledgments

This work was supported by the National Natural Science Foundation of China (Nos. 51878244 and 52170032), the the Fundamental Research Funds for the Central Universities (No. B200202101), and the Priority Academic Program Development of Jiangsu Higher Education Institutions (PAPD), China.

Appendix A Supplementary data

Supplementary material associated with this article can be found, in the online version, at doi:10.1016/j.jes.2021.11.010.

REFERENCES

Aly, R.O., Farag, R.S., Hassan, M.M, 2016. γ-Irradiation and characterization of synthesized methoxybenzylpyrimidine formimidate Schiff-base and some metal-complex derivatives. Arab. J. Chem. 9 (S1), S852–S857.

Aparna, R.S., Devi, J.S.A., Anjana, R.R., Nebu, J., George, S., 2019. Reversible Fluorescence Modulation of BSA Stabilised Copper Nanocluster for the Selective Detection of Protamine and Heparin. Analyst 144, 1799–1808.

Chakraborty, M., Mitra, I., Sarkar, K., Bardhan, M., Paul, S., Basu, S., et al., 2019. Fluorescence enhancement via aggregation effect due to microenvironmental alterations in human hemoglobin protein in presence of carbon quantum dots (CQD): Comparative spectroscopic approach. Spectrochim. Acta A. 215, 313–326.

Chen, W., Westerhoff, P., Leenheer, J.A., Booksh, K., 2003. Fluorescence excitation-emission matrix regional integration to quantify spectra for dissolved organic matter. Environ. Sci. Technol. 37 (24), 5701–5710.

Duan, L., Jiang, W., Song, Y., Xia, S., Hermanowicz, S.W, 2013. The characteristics of extracellular polymeric substances and soluble microbial products in moving bed biofilm reactor-membrane bioreactor. Bioresource Technol 148, 436–442.

Echevarria, C., Valderrama, C., Cortina, J.L., Martin, I., Arnaldos, M., Bernat, X., et al., 2019. Techno-economic evaluation and comparison of PAC-MBR and ozonation-UV revamping for organic micro-pollutants removal from urban reclaimed wastewater. Sci. Total Environ. 671, 288–298.

Fang, F., Hu, H.L., Qin, M.M., Xue, Z.X., Cao, J.S., Hu, Z.R, 2015. Effects of metabolic uncouplers on excess sludge reduction and microbial products of activated sludge. Bioresource Technol 185, 1–6.

Feng, L.J., Wang, J.J., Liu, S.C., Sun, X.D., Yuan, X.Z., Wang, S.G, 2018. Role of extracellular polymeric substances in the acute inhibition of activated sludge by polystyrene nanoparticles. Environ. Pollut. 238, 859–865.

Ganesh, K., Balraj, C., Satheshkumar, A., Elango, K.P, 2012. Spectroscopic investigation on the mechanism of formation of molecular complexes of albendazole and trimethoprim with 2,3-dichloro-5,6-dicyano-1,4-benzoquinone. Spectrochim. Acta A. 92, 46–55.

Ganesh, K., Elango, K.P, 2012. Spectroscopic and spectrofluorimetric studies on the interaction of albendazole and trimethoprim with iodine. Spectrochim. Acta A. 93, 185–197.

Habibul, N., Chen, W., 2018. Structural response of humic acid upon binding with lead: A spectroscopic insight. Sci. Total Environ. 643, 479–485.

Hernandez-Ruiz, S., Abrell, L., Wickramasekara, S., Chefetz, B., Chorover, J., 2012. Quantifying PPCP interaction with dissolved organic matter in aqueous solution: Combined use of fluorescence quenching and tandem mass spectrometry. Water Res 46 (4), 943–954.

Huangfu, X.L., Xu, Y.H., Liu, C.H., He, Q., Ma, J., Ma, C.X., et al., 2019. A review on the interactions between engineered nanoparticles with extracellular and intracellular polymeric substances from wastewater treatment aggregates. Chemosphere 219, 766–783.

Hyun-Chul, K., Dempsey, B.A, 2008. Effects of wastewater effluent organic materials on fouling in ultrafiltration. Water Res 42 (13), 3379–3384.

Jacquin, C., Lesage, G., Traber, J., Pronk, W., Heran, M., 2017. Three-dimensional excitation and emission matrix fluorescence (3DEEM) for quick and pseudo-quantitative determination of protein- and humic-like substances in full-scale membrane bioreactor (MBR). Water Res 118, 82–92.

Kavita, K., Mishra, A., Jha, B., 2013. Extracellular polymeric substances from two biofilm forming Vibrio species: characterization and applications. Carbohyd. Polym. 94 (2), 882–888.

Kimura, K., Yamato, N., Yamamura, H., Watanabe, Y., 2005. Membrane fouling in pilot-scale membrane Bioreactors (MBRs) treating municipal wastewater. Environ. Sci. Technol. 39 (16), 6293–6299.

Laspidou, C.S., Rittmann, B.E, 2002. A unified theory for extracellular polymeric substances, soluble microbial products, and active and inert biomass. Water Res 36 (11), 2711–2720.

Lee, E., Shon, H.K., Cho, J., 2014. Role of wetland organic matters as photosensitizer for degradation of micropollutants and metabolites. J. Hazard. Mater. 276, 1–9.

Li, W.-W., Yu, H.-Q, 2014. Insight into the roles of microbial extracellular polymer substances in metal biosorption. Bioresource Technol 160, 15–23.

Li, X., Wu, B., Zhang, Q., Liu, Y., Wang, J., Li, F., et al., 2020. Complexation of humic acid with Fe ions upon persulfate/ferrous oxidation: Further insight from spectral analysis. J. Hazard. Mater. 399, 123071.

Mal, J., Nancharaiah, Y.V., Bera, S., Maheshwari, N., Hullebusch, E.D.V., Lens, P.N.L, 2017. Biosynthesis of CdSe nanoparticles by anaerobic granular sludge. Environ. Sci. Nano 4 (4), 824–833.

Maruyama, T., Katoh, S., Nakajima, M., Nabetani, H., Abbott, T.P.,

Shono, A., et al., 2001. FT-IR analysis of BSA fouled on ultrafiltration and microfiltration membranes. J. Membrane Sci. 192 (1-2), 201–207.
Mei, X.J., Wang, Z.W., Xiang, Z., Fei, H., Ma, J.X., Tang, J.X., et al., 2014. Soluble microbial products in membrane bioreactors in the presence of ZnO nanoparticles. J. Membrane Sci. 451 (1), 169–176.
Mishra, A., Kavita, K., Jha, B., 2011. Characterization of extracellular polymeric substances produced by micro-algae Dunaliella salina. Carbohyd. Polym. 83 (2), 852–857.
Ng, K.K., Shi, X., Ong, S.L., Lin, C.F., Ng, H.Y, 2016. An innovative of aerobic bio-entrapped salt marsh sediment membrane reactor for the treatment of high-saline pharmaceutical wastewater. Chem. Eng. J. 295, 317–325.
Oberoi, A.S., Jia, Y., Zhang, H., Khanal, S.K., Lu, H., 2019. Insights into the Fate and Removal of Antibiotics in Engineered Biological Treatment Systems: A Critical Review. Environ. Sci. Technol. 53 (13), 7234–7264.
Ozdemir, G., Ozturk, T., Ceyhan, N., Isler, R., Cosar, T., 2003. Heavy metal biosorption by biomass of Ochrobactrum anthropi producing exopolysaccharide in activated sludge. Bioresource Technol 90 (1), 71–74.
Quang Viet, L., Nghiem, L.D., Cho, J., Maqbool, T., Hur, J, 2019. Organic carbon source-dependent properties of soluble microbial products in sequencing batch reactors and its effects on membrane fouling. J. Environ. Manage. 244, 40–47.
Raunkjær, K., Hvitved-Jacobsen, T., Nielsen, P.H, 1994. Measurement of pools of protein, carbohydrate and lipid in domestic wastewater. Water Res 28 (2), 251–262.
Sajjad, M., Kim, K.S, 2015. Influence of Mg^{2+} catalyzed granular sludge on flux sustainability in a sequencing batch membrane bioreactor system. Chem. Eng. J. 281, 404–410.
Shahriar, A., Tan, J.W., Sharma, P., Hanigan, D., Verburg, P., Pagilla, K., et al., 2021. Modeling the fate and human health impacts of pharmaceuticals and personal care products in reclaimed wastewater irrigation for agriculture. Environ. Pollut. 276, 116532.
Sheng, G.P., Yu, H.Q., Yue, Z.B, 2005. Production of extracellular polymeric substances from Rhodopseudomonas acidophila in the presence of toxic substances. Appl. Microbiol. Biot. 69 (2), 216–222.
Song, C., Sun, X.F., Xing, S.F., Xia, P.F., Shi, Y.J., Wang, S.G, 2014. Characterization of the interactions between tetracycline antibiotics and microbial extracellular polymeric substances with spectroscopic approaches. Environ. Sci. Pollut. R. 21 (3), 1786–1795.
Su, H., Xu, W., Hu, X., Xu, Y., Wen, G., Cao, Y., 2021. Spatiotemporal variations and source tracking of antibiotics in an ecological aquaculture farm in Southern China. Sci. Total Environ. 763, 143022.
Sun, X.F., Wang, S.G., Cheng, W., Fan, M.H., Tian, B.H., Gao, B.Y., et al., 2011. Enhancement of acidic dye biosorption capacity on poly(ethylenimine) grafted anaerobic granular sludge. J. Hazard. Mater. 189 (1-2), 27–33.
Thiebault, T., 2020. Sulfamethoxazole/Trimethoprim ratio as a new marker in raw wastewaters: A critical review. Sci. Total Environ. 715, 136916.
Wang, L., Wang, L., Shi, Q., Yu, H., 2018. Purification and molecular weight distribution of a key exopolysaccharide component of Bacillus megaterium TF10. J. Environ. Sci. 63, 9–15.
Wang, X.L., Li, Y., Huang, J., Zhou, Y.Z., Li, B.L., Liu, D.B, 2019. Efficiency and mechanism of adsorption of low concentration uranium in water by extracellular polymeric substances. J. Environ. Radioactiv. 197, 81–89.
Wu, M., Liang, Y., Zhang, Y., Xu, H., Liu, W., 2019. The effects of biodegradation on the characteristics and disinfection by-products formation of soluble microbial products chemical fractions. Environ. Pollut. 253, 1047–1055.
Wu, W., Duan, T., Song, H., Li, Y., Yu, A., Zhang, L., et al., 2015. The effect of continuous Ni(II) exposure on the organic degradation and soluble microbial product (SMP) formation in two-phase anaerobic reactor. J. Environ. Sci. 33, 78–87.
Xie, W.-M., Qiao, L.-L., Fang, F., Li, W.-W., Meng, H., Wang, G.-X., et al., 2019. Dynamic characteristics of soluble microbial products in a granular sludge reactor. J. Clean. Prod. 212, 576–581.
Xu, J., Hu, Y.Y., Li, X.Y., Chen, J.J., Sheng, G.P, 2018. Rapidly probing the interaction between sulfamethazine antibiotics and fulvic acids. Environ. Pollut. 243 (Pt A), 752–757.
Xu, J., Luo, H.W., Wang, Y.K., Sheng, G.P, 2015. Fluorescence approach for investigating binding properties between metals and soluble microbial products from a biological wastewater treatment plant. Process Biochem 50 (4), 636–642.
Xu, J., Sheng, G.P., Ma, Y., Wang, L.F., Yu, H.Q, 2013. Roles of extracellular polymeric substances (EPS) in the migration and removal of sulfamethazine in activated sludge system. Water Res 47 (14), 5298–5306.
Yamashita, Y., Jaffe, R., 2008. Characterizing the interactions between trace metals and dissolved organic matter using excitation-emission matrix and parallel factor analysis. Environ. Sci. Technol. 42 (19), 7374–7379.
Yang, P., Yang, M.M., Yang, B.S, 2010. Fluorescence enhancement effect and the interaction between donor and acceptor. Chinese J. Chem. 14 (2), 109–113.
Yang, W., Wang, J., Hua, M., Zhang, Y., Shi, X., 2018. Characterization of effluent organic matter from different coking wastewater treatment plants. Chemosphere 203, 68–75.
Zhao, J., Wang, Z.Y., White, J.C., Xing, B.S, 2014. Graphene in the Aquatic Environment: Adsorption, Dispersion, Toxicity and Transformation. Environ. Sci. Technol. 48 (17), 9995–10009.
Zhou, L., Zhuang, W., Wang, X., Yu, K., Yang, S., Xia, S., 2017a. Potential acute effects of suspended aluminum nitride (AlN) nanoparticles on soluble microbial products (SMP) of activated sludge. J. Environ. Sci. 57, 284–292.
Zhou, Z.B., He, X., Zhou, M.H., Meng, F.G, 2017b. Chemically induced alterations in the characteristics of fouling-causing bio-macromolecules - Implications for the chemical cleaning of fouled membranes. Water Res 108, 115–123.
Zumstein, M.T., Helbling, D.E, 2019. Biotransformation of antibiotics: Exploring the activity of extracellular and intracellular enzymes derived from wastewater microbial communities. Water Res 155, 115–123.